



Geophysical Research Letters

RESEARCH LETTER

10.1029/2018GL079424

Key Points:

- Very high amplitude radio pulses sometimes occur at either the very beginning or the very end of downward negative leaders
- They are produced at altitudes either near 6 or <1 km, suggesting they both occur in high-electric field regions in the cloud and near the ground
- We conjecture that these pulses may be signatures of downward TGFs associated with negative leaders propagating in high-field regions

Correspondence to:

S. A. Cummer,
cummer@ee.duke.edu

Citation:

Lyu, F., & Cummer, S. A. (2018). Energetic radio emissions and possible terrestrial gamma-ray flashes associated with downward propagating negative leaders. *Geophysical Research Letters*, 45. <https://doi.org/10.1029/2018GL079424>

Received 3 JUL 2018

Accepted 25 SEP 2018

Accepted article online 1 OCT 2018

Energetic Radio Emissions and Possible Terrestrial Gamma-Ray Flashes Associated With Downward Propagating Negative Leaders

Fanchao Lyu¹  and Steven A. Cummer¹ 

¹Electrical and Computer Engineering Department, Duke University, Durham, NC, USA

Abstract A study of negative polarity energetic in-cloud pulses (–EIPs) during thunderstorms reveals that –EIPs occur during two distinct stages of downward negative leader development. The first group is observed at the beginning of downward negative leaders, with estimated average source altitude of ~5.9 km between main negative and lower positive charge regions. The second and new group are observed at the very end of downward negative leaders and appear to be produced at low altitudes close to the ground, where image charges amplify the electric field between the leader tip and conducting ground. Negative EIPs appear to occur only in these two scenarios, suggesting that their production require a high background electric field. Their radio emission signatures and occurrence contexts are similar with +EIPs, which are known to be connected to terrestrial gamma-ray flashes. We thus suggest that these two types of –EIPs may be associated with downward terrestrial gamma ray flashes.

Plain Language Summary Studies of especially powerful lightning events provide important insights into the physics of lightning and associated processes. It was recently established that there are three different lightning processes that produce the most powerful electric currents: cloud-to-ground strokes, narrow bipolar events, and the newly identified energetic in-cloud pulses (EIPs). Positive polarity EIPs, produced by lightning propagating upward inside a cloud, are closely linked to terrestrial gamma ray flashes (TGFs), which are bursts of high-energy radiation whose origins remain only partly understood. Here we have now identified two classes of negative polarity EIPs that are produced when lightning channels are traveling downward toward the ground, with one occurred in the clouds and the other one appeared to be produced at low altitudes close to the ground. These two new types of EIP are produced in the same physical scenario as positive EIPs, when a lightning channel encounters a region of high-electric field. We thus conjecture that negative EIPs are associated with rarely seen downward TGFs that emit high-energy radiation toward the ground. This discovery provides a new way to measure and investigate downward TGFs from distant radio emissions alone.

1. Introduction

Measurements of radio emissions during lightning discharges, especially for some classes of energetic events, provide important insight into the understanding of lightning processes and associated phenomena. By analyzing high peak current in-cloud lightning events, a new class of lightning event called energetic in-cloud pulses (EIPs) was identified, which occurs during negative leader propagation and is clearly distinct from narrow bipolar events and cloud-to-ground (CG) return strokes (Lyu et al., 2015). From their temporal occurrence context, the more common positive (+) EIPs occur during ascending negative in-cloud leaders, while rarer negative (–) EIPs were identified that occur shortly after the initiation of downward negative CG leaders (Lyu et al., 2015). From the analysis on the simultaneous measurements of +EIPs by ground-based radio sensors, lightning mapping arrays (Rison et al., 1999), and Fermi Gamma-ray Burst Monitor (Briggs et al., 2010), +EIPs were now shown to be closely linked to a subset of terrestrial gamma ray flashes (TGFs; Cummer et al., 2017; Lyu et al., 2016), which suggests most and maybe all +EIPs are associated with TGFs, and thus providing a novel way to detect and investigate a subset of TGFs from distant radio emissions.

Significantly less is known about –EIPs. Previously, Lyu et al. (2015) reported three –EIPs that were produced just after the initiation of downward negative leaders. Based on the similar (but

upside-down) occurrence context of +EIPs and these few –EIPs, Lyu et al. (2016) suggested that –EIPs are linked to TGFs in the same way that +EIPs are known to be. However, the source positions, which is important for either –EIPs or their possible associated TGFs, were still unclear. Our goal in this study is a more comprehensive search for and analysis of high peak current lightning processes during downward negative leaders. Following the approach taken in previous investigations (Lyu et al., 2015, 2016), we report here that there are in fact two classes of –EIPs that occur in distinct stages of downward negative leader propagation.

Briefly, –EIPs are produced either less than 1 ms after the initiation of a downward negative leader (as reported by Lyu et al., 2015) or a short time (usually less than ~ 1 ms) before a negative leader contacts the ground in a first –CG stroke (to our knowledge not previously reported). The source height of the first type was estimated for the first time in this study, which occurs at an average source altitude of 5.9 km when the downward negative leader tip is still between the main negative and lower positive cloud charge regions. The second type was estimated to usually occur at ~ 1 -km altitude or lower, when the image charge proximity can significantly amplify the electric field between the leader tip and ground. That –EIPs are seen only in these two high-field scenarios suggests a strong connection to +EIPs, which are known to occur when ascending negative leaders are in the high-field region between the main negative and upper positive thunderstorm charge layers (Lyu et al., 2015). It has also been shown that +EIPs are likely and perhaps always associated with TGFs (Cummer et al., 2017; Lyu et al., 2016). Based on the apparent similarity in the physical origins of all EIPs, we conjecture that these two types of –EIPs, one type occurring at cloud altitudes and the other occurring close to the ground, may be also associated with downward TGFs, although more research and measurements are needed to fully understand their possible connection.

2. Instruments and Data Set

This study employs multiband magnetic field measurements of lightning radio emissions at low frequency (LF, ~ 1 –300 kHz), very low frequency (VLF, 50 Hz to ~ 30 kHz), and ultralow frequency (ULF, < 1 –400 Hz). Six LF sensors were deployed in Durham, NC (Duke); Melbourne, FL (FIT); Oxford, MS (Miss); Norman, OK (OU); Manhattan, KS (KSU); and Lubbock, TX (TTU). The VLF and ULF sensors were deployed in Durham, NC. Data from the National Lightning Detection Network (NLDN), operated by Vaisala Inc. (Cummins & Murphy, 2009; Cummins et al., 1998), were used to identify the time and location of lightning events of interest.

As in previous studies of EIPs (Lyu et al., 2015, 2016), we started with NLDN reports to identify high peak current lightning events. All lightning events, regardless of NLDN classification and polarity, during the years 2015 and 2016 with peak current above 150 kA and within 1,000 km (this range was extended to 1,500 km in 2016) from one of our LF sensors were examined in detail. These events were classified (CG or narrow bipolar event or EIP and polarity) based on the broadband radio signals from the LF, VLF, and ULF radio sensors using specific quantitative signal criteria (primarily pulse duration and isolation from other emissions) that are described in full detail by Lyu et al. (2015).

A total of 876 EIPs emerged from this data set. Eight hundred fifty-three of these were +EIPs with characteristics consistent with those reported previously by Lyu et al. (2015). We presume that most or all of these are also TGFs as found by Lyu et al. (2016). There were also 23 –EIPs that produced unambiguously negative polarity LF/VLF signals. Although –EIPs with peak current above 150 kA are clearly rare, we find from these 23 that –EIPs can be clearly classified into two types based on the stage of downward leader development when they are produced.

The first type consists of 18 –EIPs that have exactly the same characteristics with the three –EIPs reported by Lyu et al. (2015), with NLDN-reported peak current magnitudes ranging from 151 to 248 kA. This type of –EIP occurs less than 1 ms after the initiation of a downward negative leader. Some of these downward negative leaders eventually contact the ground in a negative CG stroke, and some do not. All of these –EIPs occur during the so-called preliminary breakdown (PB) stage of negative leader development (Clarence & Malan, 1957; Rakov & Uman, 2003) and are thus referred as PB-type or early –EIPs. The source height of –EIPs was measured, for the first time, and found to be ~ 5.9 km. Together with supporting meteorological measurements, we confirm that PB-type –EIPs are produced when the leader tip is still between the main negative and the lower positive charge regions.

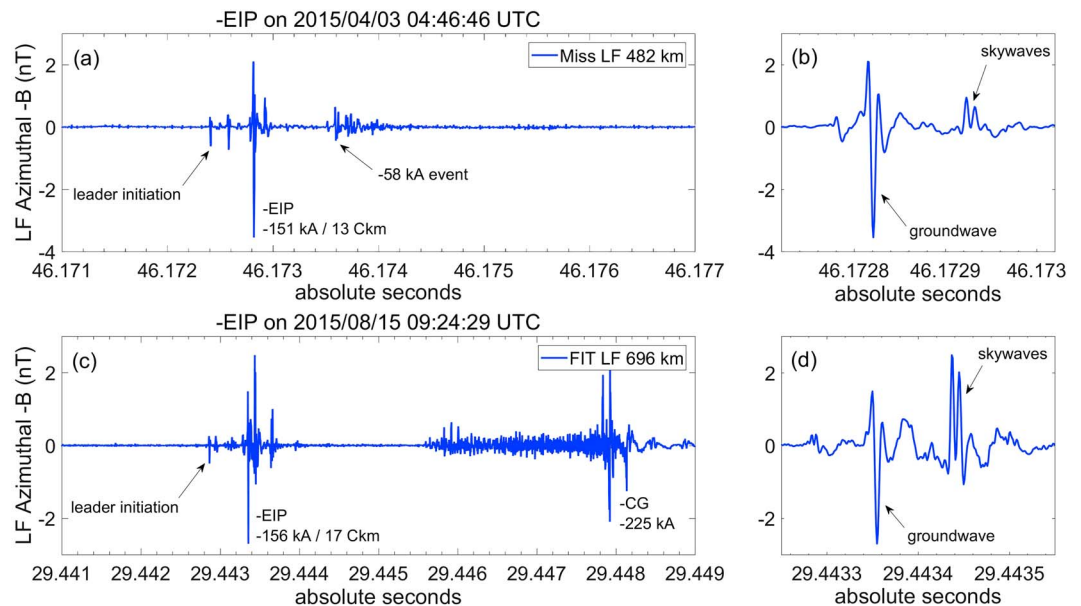


Figure 1. LF signals from two occurrence contexts of PB-type –EIPs. (a) An –EIP occurs 400 μ s after leader initiation and is followed by a short duration leader pulse train that ends before any CG occurs. (b) A shorter time window shows the –EIP groundwave and the sky wave pair. (c) An –EIP occurs again 400 μ s after leader initiation and is followed by a stepped leader pulse train that ends as a high peak current return stroke. (d) Similar to (b) for the –EIP in (c). LF = low frequency; EIP = energetic in-cloud pulse; Miss = Oxford, MS; FIT = Melbourne, FL; CG = cloud-to-ground.

The second type of –EIP, which to our knowledge has not been previously reported, also occurs during downward negative leader propagation. However, 4 of 5 of this second type of –EIP occur less than 1.1 ms (one occurs at 3.9 ms) before a first –CG return stroke (RS) and thus are produced when the leader has propagated almost to the ground. We thus refer to these as PreRS-type or late –EIPs.

In the following sections, we will show the basic phenomenology of the two types of –EIPs, including the radio emission signature, occurrence contexts, and the estimated source altitudes.

3. Early PB-Type –EIPs

3.1. Temporal Occurrence Contexts of Early PB-type –EIPs

Figure 1 shows two PB-type –EIPs in LF radio emissions recorded 500 to 700 km away. Like +EIPs (Lyu et al., 2015), all the PB-type –EIPs were both preceded and followed by smaller LF pulses within a roughly 1-ms window. This shows that lightning activity and leader development occur before and after the PB-type –EIPs. All 18 PB-type –EIPs analyzed here occurred approximately 0.5 ms after the leader initiation and have a pulse duration of approximately 30 μ s. As illustrated in Figure 1, PB-type –EIPs are always followed by further downward leader development and sometimes end in a high peak current –CG stroke. However, some PB-type –EIPs (7 of the 18) are followed by leader development that terminates before ground contact. This confirms that PB-type –EIPs are produced by the conditions of or encountered by the leader soon after initiation and have little to do with what the leader does later.

Figure 1a illustrates a PB-type –EIP that was not followed by a –CG stroke. The –151-kA –EIP occurred approximately 0.4 ms after the leader initiation and was followed by a 0.8-ms pulse train likely produced by further negative leader propagation. The pulse train included a –58-kA in-cloud lightning event which was 0.4 km horizontally from the –EIP. Figure 1c shows another PB-type –EIP that was followed by a strong –CG stroke. Similar to the –EIP in Figure 1a, the –156-kA –EIP occurred approximately 0.4 ms after the leader initiation. After a delay of about 1.5 ms, the negative downward stepped leader continued, and 4.5 ms after the –EIP, the downward leader terminated with a –225-kA CG return stroke that was horizontally 1.4 km from the –EIP.

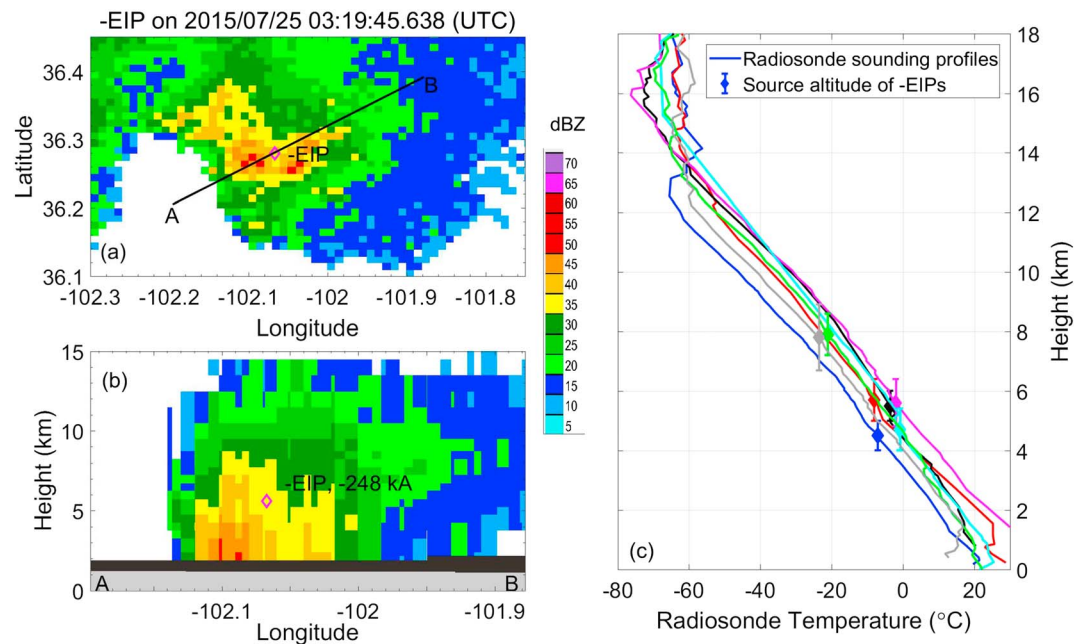


Figure 2. Parts (a) and (b) show radar scans for the PB-type –EIP at 03:19:45.638 UTC on 25 July 2015. Composite reflectivity reveals the highest reflectivity in all echoes and was used in the plan view map in (a). (c) The radiosonde temperature close to the –EIP-producing thunderstorms and the source altitude of –EIPs. Seven different color lines plot the radiosonde temperature from the station and time close to seven different PB-type –EIP producing storms, while the diamonds plot the heights of these seven –EIPs on the temperature plots, with source height estimated error of 0.5 to 1.1 km for these seven –EIPs shown by the error bar along the diamond plots. EIP = energetic in-cloud pulse.

3.2. Source Altitude of PB-type –EIPs

For an elevated radio emission source, the source altitude can be estimated from the time difference of two identifiable sky waves reflected between earth and ionosphere (Smith et al., 2004). Here we report the source altitude of PB-type –EIPs for the first time.

As shown in Figures 1b and 1d, the LF waveforms from two PB-type –EIPs at distances of 482 and 696 km from the sensors show two sky wave pulses following the ground wave. From pulse time separation, these two –EIPs were estimated to occur at 4.5 ± 0.5 and 5.2 ± 0.6 km above ground level. The sky wave reflections are clearly identifiable in LF waveforms from another six PB-type –EIPs. Together, these eight PB-type –EIPs occurred at altitudes from 4.5 to 7.9 km, with a mean altitude of 5.9 km. This is consistent with the altitude of initial breakdown pulses during normal CG flashes as measured from different lightning mapping arrays (Bitzer et al., 2013; Karunarathne et al., 2013; Lyu et al., 2014). This source altitude indicates the PB-type –EIPs occur when the existing leader is still between the main negative and lower positive charge regions.

Meteorological measurements also show that PB-type –EIPs occur between the main negative and lower positive thunderstorm charge regions. Figures 2a and 2b show the plan and vertical views of the radar echo from at KAMA radar, Amarillo, TX, near the time of one –EIP on 25 July 2015, 03:19:45.638 UTC, with the NLDN reported peak current of –248 kA. The source altitude was estimated at 5.6 ± 0.8 km from the sky wave analysis. It was located 121 km from the KAMA radar. The –EIP was located within the 35-dBZ echo region, which is considered to be strong convection region during thunderstorms. The vertical radar echo map along the line AB in Figure 2b showed that the storm echo top was up to 15 km, while the radiosonde data nearby showed that the zero-degree temperature level was around 5.3 km. This indicates a possible lower positive charge region lower than 5-km altitude and a main negative charge region above 6 km (Stolzenburg & Marshall, 2009). The 5.6-km –EIP source altitude is thus between the main negative charge region and the lower positive charge region.

Figure 2c shows the source altitudes of seven PB-type –EIPs overlaid on the radiosonde temperature from observation stations close to the –EIP-producing thunderstorms both in time and space domains. Two PB-

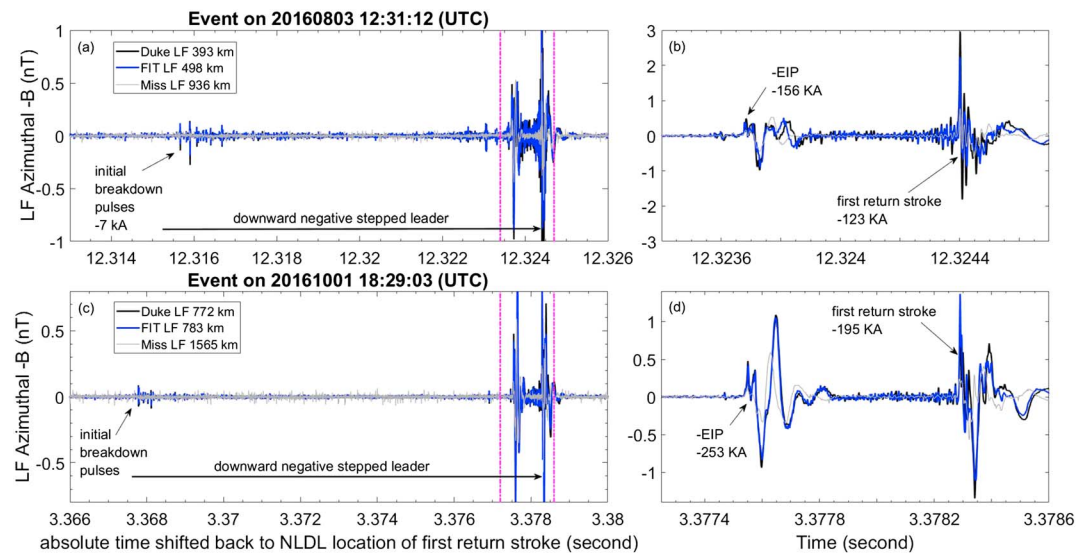


Figure 3. Two examples of the PreRS-type $-EIP$. (a) A PreRS-type $-EIP$ from the $-CG$ flash on 03 August 2016 at 12:31:12 (UTC). The times of the LF signals from three LF sensors deployed at Duke, FIT, and Miss were shifted back to the NLDN reported location of the CG stroke. (b) A zoom-in plot of the LF signals during a 1.3-ms window marked by the two dashed lines in (a). (c) and (d) Same as (a) and (b) another PreRS-type $-EIP$ that occurred on 01 October 2016 at 18:29:03 (UTC). The time alignment of the $-EIP$ and $-CG$ signals from different sensors indicates they originated very close to each other. LF = low frequency; Duke = Durham, NC; FIT = Melbourne, FL; Miss = Oxford, MS; EIP = energetic in-cloud pulse; CG = cloud-to-ground. NLDN = National Lightning Detection Network.

type $-EIP$ s were estimated in the region with radiosonde sounding temperature around $-20^{\circ}C$, and the other five PB-type $-EIP$ s occurred in the region with temperature between -10 and $0^{\circ}C$. Generally, a main negative charge center is around $-20^{\circ}C$ and may vary slightly in different kind of thunderstorm systems with stronger or weaker updrafts, while a possible main positive charge center can be expected where the temperature is above $0^{\circ}C$ (Stolzenburg & Marshall, 2009).

The estimated source altitude and the thunderstorm meteorological conditions indicate that the PB-type $-EIP$ s occurred in the region between the main negative and the lower positive charge regions. PB-type $-EIP$ s are produced within 0.5 ms of the negative leader initiation in a location where a strong electric field could exist. Except for different charge layers being involved, this is exactly the same scenario as that for $+EIP$ production, which occurs when a propagating negative leader (upward for $+EIP$ s) is between the main negative and upper positive charge layers (Cummer et al., 2014; Lyu et al., 2015), a region where local electric fields are also likely to be high.

4. Late PreRS-Type $-EIP$ s

Five late PreRS-type $-EIP$ s that occurred much later in the development of a downward CG leader were found in this study. The radio emission signature of the PreRS-type $-EIP$ s is definitely distinct from those of return strokes, as shown in Figure 3. Figures 3a and 3b illustrate one that occurred on 03 August 2016 at 12:31:12 UTC. From the LF radio data, the negative leader initial breakdown pulses began at of 12.315 s, which was 8.9 ms before the first return stroke. During the development downward stepped leader, the $-EIP$ occurred 0.7 ms before the CG stroke. The $-EIP$ and $-CG$ had NLDN peak currents of -156 and -134 kA, respectively, and were separated horizontally by only 150 m according to the NLDN locations. One initial breakdown pulse reported by NLDN occurred at 12.315 s with peak current of -7 kA and was located horizontally 4.74 km from $-EIP$. This $-EIP$ occurred spatially close to the $-CG$ return stroke, rather than in the initiation region where initial breakdown pulses and PB-type $-EIP$ s occurred. The continuous propagation of the downward negative leader both before and after the PreRS-type $-EIP$ and the first return stroke can be seen from the pulse-like emission.

Another PreRS-type $-EIP$ occurred on 01 October 2016 at 18:29:03 (UTC) and is shown in Figure 3c. Two events were reported by NLDN with peak currents of -253 kA (the $-EIP$) and -195 kA (the $-CG$),

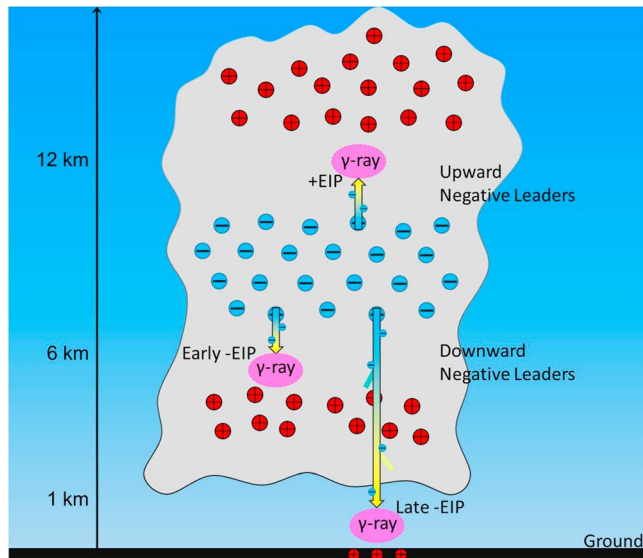


Figure 4. Schematic of the positions of both positive and two types of negative EIPs (early PB-type and late PreRS-type) during the propagation of negatively charged lightning leaders (yellow arrows showing the current position and direction) and their possible association of gamma-ray emissions (the magenta area). EIP = energetic in-cloud pulse.

separated by 1.6 km horizontally. The relatively large 50% geolocation error of 500 m indicates that these may have been much closer. As shown in Figures 3c and 3d, while the entire downward negative leader development lasted 10.5 ms, the $-$ EIP occurred only 0.7 ms ahead of the CG return stroke, which is consistent with the case in Figure 3a.

Another three PreRS-type $-$ EIPs were produced in nearly the same contexts as the above two cases shown in Figure 3, with NLDN reported peak currents of -302 , -190 , and -209 kA. They occurred 0.25, 3.9, and 1.1 ms before the first return stroke, with overall leader durations of 9.4, 11.3, and 8.3 ms, respectively. The one that occurred 3.9 ms before the return stroke is an outlier as the remaining four all had time gaps less than 1.1 ms. No source altitudes for the PreRS-type $-$ EIPs can be directly obtained from the LF waveforms because the detectable sky waves do not have two distinct reflections. This suggests a relatively low-source altitude. Assuming a relatively fast downward propagation speed of the downward negative stepped leaders of $5\text{--}10 \times 10^5$ m/s (Rakov & Uman, 2003, pp. 123) and time separation of ~ 1 ms, four of these PreRS-type $-$ EIPs likely occurred only $\sim 0.5\text{--}1$ km above the ground. The one outlier occurred 3.9 ms before the CG return stroke. With total leader duration of 11.3 ms, this PreRS-type $-$ EIP was still produced relatively late in the development of the leader. If this leader propagated at the slow end of this range (5×10^5 m/s), the source height still would be a relatively low 2 km. PB-type and PreRS-type $-$ EIPs are thus distinct populations that occur in entirely different stages of

downward negative leader development. Technically speaking, at 1-km altitude, these PreRS-type $-$ EIPs are probably not in-cloud anymore. But the term in-cloud is often applied to any lightning process that does not involve ground or grounded object interaction, and given the waveform similarity across all types of EIP, we prefer to apply the term EIP to all of these events.

Although the PreRS-type $-$ EIPs are generated during the downward negative leaders, their LF radio signals show some features that are distinct from the normal negative stepped leader pulses. The five PreRS-type $-$ EIPs reported here had pulse durations of 75 to 90 μ s, with mean value of 83 μ s, which is more than five times longer than the duration of normal stepped leader pulses (usually ~ 10 μ s by our measurement). In addition, the PreRS-type $-$ EIPs usually exhibited a slow rising edge with small subpeaks superimposed on it or sometimes with multiply peaked initial pulses, as the $-$ EIPs shown in Figure 3. Both signatures are distinct from the normal negative stepped leader pulse, but entirely consistent with the $+EIPs$ (Lyu et al., 2015, 2016), further suggesting some relationship between them. Moreover, it is also clear that the LF radio signatures of PreRS-type $-$ EIPs are distinct with that of the following return stroke, suggesting some fundamental differences between them despite their comparably high peak currents.

5. Discussion and Conclusions

Radio emissions from NLDN reported high peak current lightning events (above 150 kA) during downward negative leaders were investigated in detail. Two classes of energetic events that are generated at two very different stages of the downward negative leader development were identified. One, the early PB-type $-EIP$, occurs very quickly (within 0.5 ms) after initiation of a downward negative leader. The other, the late PreRS-type $-EIP$, occurs at the very end of the downward leader development and usually less than 1 ms before the leader contacts the ground and forms a CG return stroke. The extremely high peak NLDN peak currents and the tens of microsecond time scale indicate that $-EIPs$ are just as capable of producing nonlinear ionosphere perturbations and optical emissions in the form of elves as CG strokes (Inan et al., 1991, 2010; Marshall et al., 2010) and $+EIPs$ and TGFs (Liu et al., 2017).

The sky wave ionospheric reflections from PB-type $-EIPs$ enable us to estimate their altitude for the first time. We find source altitudes between 4.5 and 7.9 km (mean value of 5.9 km), which is consistent with their occurrence less than a millisecond after downward leader initiation. The radar echo and radiosonde records show that PB-type $-EIPs$ were located within 35-dBZ region and at the levels with temperature between -25 $^{\circ}$ C

and 0 °C. This establishes that PB-type –EIPs are produced in a region between the main negative and the lower positive charge layers. In contrast, the temporal and spatial context of the PreRS-type –EIPs is totally different. The short (usually < 1 ms) separation between these PreRS-type –EIPs and a first CG return stroke indicates they are produced when the negative leaders are close to the ground, with an estimated source altitude of 0.5–1 km above the ground for 4 of the 5 cases analyzed here.

Despite the differences in where +EIPs and the two classes of –EIPs are produced, many aspects of them are similar. They are all associated with propagating negative leaders, either upward (+EIPs) or downward (–EIPs). Beyond the polarity difference, the basic features of the LF waveforms they produce are essentially the same. They all have pulse durations of approximately 30 to 100 μ s, and multiple peaks of the initial pulse are not uncommon. This suggests that the nature and magnitude of the current and charge motion producing both +EIPs and –EIPs are similar, regardless of where they are produced.

These similarities further suggest they may have a common physical origin. We conjecture that all types of EIPs are produced when negative leaders of sufficient length propagate through a high local electric field region. Previous work has shown that +EIPs are generated a few milliseconds after upward in-cloud negative leader initiation, when the leader is between the main negative and upper positive charge layers (Cummer et al., 2014; Lyu et al., 2015). This is one region where negative leaders are expected to encounter high-electric fields. We have shown here that PB-type –EIPs occur when recently initiated downward negative leaders are still between the main negative and lower positive charge regions, which is another region where negative leaders can encounter high-electric fields. Lastly, we have identified here for the first time Pre-RS-type –EIPs, which occur when downward negative leader is approximately 1 km above the ground. In this location, the ground image charge is close enough to the leader tip to produce a high-electric field. The existence of a high-electric field associated with the propagation of the downward negative leader is also suggested by the large peak current of the following first return stroke. All the first CG return strokes followed by the PreRS-type –EIPs were also reported by NLDN with large peak currents, ranging from –123 to –207 kA (with mean value of –170 kA) for five –EIPs in this study. The unusual and atypical nature of the downward leaders that produce PreRS-type –EIPs is clearly shown by the rarity of these events (only five found in 2 years). It may well be unusual circumstances such as a minimally branched leader that is responsible for producing them.

That EIPs are only observed in these three scenarios indicates that a high background electric field may be a necessary condition for producing EIPs. The overwhelming majority of negative leaders do not produce EIPs, however, and thus there may well be other required conditions beyond the possibility of high background electric field. But we emphasize that our search for EIPs includes an extremely high peak current threshold, and thus whatever process produces EIPs occurs more often than the small numbers reported here indicate.

This similarity in the physical origins of all EIPs has at least one important possible implication as discussed below. +EIPs during upward negative leaders have been shown to be strongly linked to a subset of Fermi Gamma-ray Burst Monitor TGFs (Cummer et al., 2014; Lyu et al., 2016) and most and maybe all +EIPs are also TGFs (Cummer et al., 2017). We propose the possibility that most and maybe all –EIPs are also TGFs, although these are directed downward because of the reversed electric field direction. TGFs associated with +EIPs appear to be driven by strong background in-cloud electric fields, aided by additional field enhancement from the long leader channel and perhaps also by transient leader tip fields (Celestin et al., 2012; Dwyer, 2012; Liu & Dwyer, 2013; Pasko, 2014). We speculate that essentially the same combination of conditions could also be encountered by negative leaders when –EIPs are produced, and thus, it is entirely possible that most if not all are also downward-directed TGFs, although additional observations would be required and highly beneficial.

A schematic illustrating the electrically similar positions of both positive and negative EIPs and their possible association of gamma-ray emissions, known and presumed, during the propagation of negative leaders is illustrated in Figure 4. The similar amplitude of all types of EIP indicates that the brightness of the conjectured downward TGFs associated with –EIPs is comparable to the known brightness of upward, satellite-detected TGFs associated with +EIPs. TGFs weaker by several orders of magnitude associated with downward negative leaders have been recently reported (Abbasi et al., 2018). These weak TGFs occurred within 1–2 ms of the downward leader initiation and do have an association with radio pulses during the leader development. Although the occurrence context of these weak TGFs does not appear to be as specific as that for the –EIPs reported here, the findings of Abbasi et al. (2018) show that weak gamma-ray production can occur

during downward negative leaders, and it is possible that gamma-ray production can occur much more strongly under the high-electric field conditions associated with $-EIPs$ that we find here. This possible connection between $-EIPs$ and TGFs requires further research, but the possibility we proposed here can help guide future ground-based TGF detection experiments and also identifies several different physical scenarios whose TGF-generation potential can be explored in numerical simulations.

Acknowledgments

The authors would like to acknowledge support from the National Science Foundation Dynamic and Physical Meteorology program through grant AGS-1565606 and the Defense Advanced Research Projects Agency (DARPA) Nimbus program through grant HR0011-10-1-0059. This work complies with the AGU data policy. The authors also would like to thank University of Wyoming to provide the atmospheric sounding data, which is available at <http://weather.uwyo.edu/upperair/sounding.html>. The radar data are available at <https://www.ncdc.noaa.gov/nexradinv/map.jsp>. The LF data presented in this study are available at Duke Digital Repository (<https://doi.org/10.7924/r4j963v4s>).

References

- Abbasi, R., Abu-Zayyad, T., Allen, M., Barcikowski, E., Belz, J. W., Bergman, D. R., et al. (2018). Gamma-ray showers observed at ground level in coincidence with downward lightning leaders. *Journal of Geophysical Research: Atmospheres*, *123*, 6864–6879. <https://doi.org/10.1029/2017JD027931>
- Bitzer, P. M., Christian, H. J., Stewart, M., Burchfield, J., Podgorny, S., Corredor, D., et al. (2013). Characterization and applications of VLF/LF source locations from lightning using the Huntsville Alabama Marx Meter Array. *Journal of Geophysical Research: Atmospheres*, *118*, 3120–3138. <https://doi.org/10.1002/jgrd.50271>
- Briggs, M. S., Fishman, G. J., Connaughton, V., Bhat, P. N., Paciesas, W. S., Preece, R. D., et al. (2010). First results on terrestrial gamma ray flashes from the Fermi Gamma-ray Burst Monitor. *Journal of Geophysical Research*, *115*, A07323. <https://doi.org/10.1029/2009JA015242>
- Celestin, S., Xu, W., & Pasko, V. P. (2012). Terrestrial gamma ray flashes with energies up to 100 MeV produced by nonequilibrium acceleration of electrons in lightning. *Journal of Geophysical Research*, *117*, A05315. <https://doi.org/10.1029/2012JA017535>
- Clarence, N. D., & Malan, D. J. (1957). Preliminary discharge processes in lightning flashes to ground. *Quarterly Journal of the Royal Meteorological Society*, *83*, 161–172.
- Cummer, S. A., Briggs, M. S., Dwyer, J. R., Xiong, S., Connaughton, V., Fishman, G. J., et al. (2014). The source altitude, electric current, and intrinsic brightness of terrestrial gamma ray flashes. *Geophysical Research Letters*, *41*, 8586–8593. <https://doi.org/10.1002/2014GL062196>
- Cummer, S. A., Lyu, F., Briggs, M. S., Cramer, E., Stanbro, M., Roberts, O., & Smith, D. M. (2017). The connection between terrestrial gamma-ray flashes and energetic in-cloud lightning pulses, presented at 2017 Fall Meeting, AGU, New Orleans, 11–15 Dec.
- Cummins, K. L., & Murphy, M. J. (2009). An overview of lightning location systems: History, techniques, and data uses, with an in-depth look at the U. S. NLDN. *IEEE Transactions on Electromagnetic Compatibility*, *51*(3), 499–518. <https://doi.org/10.1109/TEMC.2009.2023450>
- Cummins, K. L., Murphy, M. J., Bardo, E. A., Hiscox, W. L., Pyle, R. B., & Pifer, A. E. (1998). A combined TOA/MDF technology upgrade of the U.S. National Lightning Detection Network. *Journal of Geophysical Research*, *103*, 9035–9044. <https://doi.org/10.1029/98JD00153>
- Dwyer, J. R. (2012). The relativistic feedback discharge model of terrestrial gamma ray flashes. *Journal of Geophysical Research*, *117*, A02308. <https://doi.org/10.1029/2011JA017160>
- Inan, U. S., Bell, T. F., & Rodriguez, J. V. (1991). Heating and ionization of the lower ionosphere by lightning. *Geophysical Research Letters*, *18*, 705–708. <https://doi.org/10.1029/91GL00364>
- Inan, U. S., Cummer, S. A., & Marshall, R. A. (2010). A survey of ELF and VLF research on lightning-ionosphere interactions and causative discharges. *Journal of Geophysical Research*, *115*, A00E36. <https://doi.org/10.1029/2009JA014775>
- Karunarathne, S., Marshall, T. C., Stolzenburg, M., Karunarathna, N., Vickers, L. E., Warner, T. A., & Orville, R. E. (2013). Locating initial breakdown pulses using electric field change network. *Journal of Geophysical Research: Atmospheres*, *118*, 7129–7141. <https://doi.org/10.1002/jgrd.50441>
- Liu, N. Y., & Dwyer, J. R. (2013). Modeling terrestrial gamma ray flashes produced by relativistic feedback discharges. *Journal of Geophysical Research: Space Physics*, *118*, 2359–2376. <https://doi.org/10.1002/jgra.50232>
- Liu, N. Y., Dwyer, J. R., & Cummer, S. A. (2017). Elves accompanying terrestrial gamma ray flashes. *Journal of Geophysical Research: Space Physics*, *122*, 10,563–10,576. <https://doi.org/10.1002/2017JA024344>
- Lyu, F., Cummer, S. A., Briggs, M., Marisaldi, M., Blakeslee, R. J., Bruning, E., et al. (2016). Ground detection of terrestrial gamma ray flashes from distant radio signals. *Geophysical Research Letters*, *43*, 8728–8734. <https://doi.org/10.1002/2016GL070154>
- Lyu, F., Cummer, S. A., & McTague, L. (2015). Insights into high peak current in-cloud lightning events during thunderstorms. *Geophysical Research Letters*, *42*, 6836–6843. <https://doi.org/10.1002/2015GL065047>
- Lyu, F., Cummer, S. A., Solanki, R., Weinert, J., McTague, L., Katko, A., et al. (2014). A low-frequency near-field interferometric-TOA 3-D Lightning Mapping Array. *Geophysical Research Letters*, *41*, 7777–7784. <https://doi.org/10.1002/2014GL061963>
- Marshall, R. A., Inan, U. S., & Glukhov, V. S. (2010). Elves and associated electron density changes due to cloud-to-ground and in-cloud lightning discharges. *Journal of Geophysical Research*, *115*, A00E17. <https://doi.org/10.1029/2009JA014469>
- Pasko, V. P. (2014). Electrostatic modeling of intracloud stepped leader electric fields and mechanisms of terrestrial gamma ray flashes. *Geophysical Research Letters*, *41*, 179–185. <https://doi.org/10.1002/2013GL058983>
- Rakov, V. A., & Uman, M. A. (2003). *Lightning-physics and effects*. New York: Cambridge University Press. <https://doi.org/10.1017/CBO9781107340886>
- Rison, W., Thomas, R. J., Krehbiel, P. R., Hamlin, T., & Harlin, J. (1999). A GPS-based three-dimensional lightning mapping system: Initial observations in central New Mexico. *Geophysical Research Letters*, *26*, 3573–3576. <https://doi.org/10.1029/1999GL010856>
- Smith, D. A., Heavner, M. J., Jacobson, A. R., Shao, X. M., Massey, R. S., Sheldon, R. J., & Wiens, K. C. (2004). A method for determining intracloud lightning and ionospheric heights from VLF/LF electric field records. *Radio Science*, *39*, RS1010. <https://doi.org/10.1029/2002RS002790>
- Stolzenburg, M., & Marshall, T. C. (2009). Electric field and charge structure in lightning-producing clouds. In H.-D. Betz, U. Schumann, & P. Laroche (Eds.), *Lightning: Principles, instruments and applications* (pp. 59–60). Netherlands: Springer. https://doi.org/10.1007/978-1-4020-9079-0_3